Chaotic Behavior of Deterministic Systems

Generally deterministic responses are expected when deterministic system are subjected to deterministic excitations, and random excitations are expected when the inputs are random processes. However, it has been shown that many nonlinear systems with or without deterministic excitations under certain conditions produce seemingly random responses. Such bounded nonperiodic, apparently random motions have been called "chaotic motions." Fourier analysis of these responses shows a broad spectrum of frequencies in spite of the fact that the excitations are of a single frequency. In this section, a few examples of chaotic response of simple dynamical systems are presented.

***Example 1*: Duffing Oscillator** (Y. Ueda in "New Approaches to Nonlinear Problems in Dynamics," Ed. P.J. Holmes, SIAM (1980).

Consider a Duffing oscillator

$$\frac{d^2x}{dt^2} + k\frac{dx}{dt} + x^3 = B\cos t$$

or

$$\frac{dx}{dt} = y$$

$$\frac{dy}{dt} = -ky - x^3 + B\cos t$$

Numerical solution to the Duffing equation shows for certain range of values for k and B, the response becomes chaotic (Ueda, 1980). Figure 1, shows the Poincare map for chaotic responses of the Duffing oscillator. Figure 2 shows trajectories of various steady motions in the phase plane for different values of parameters. The corresponding time histories are shown in Figure 3.

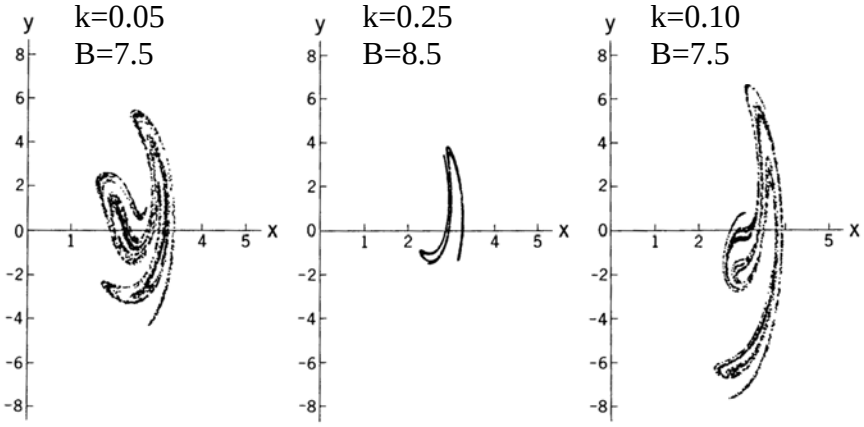

Figure 1. Poincare map for chaotic responses of Duffing's oscillator.

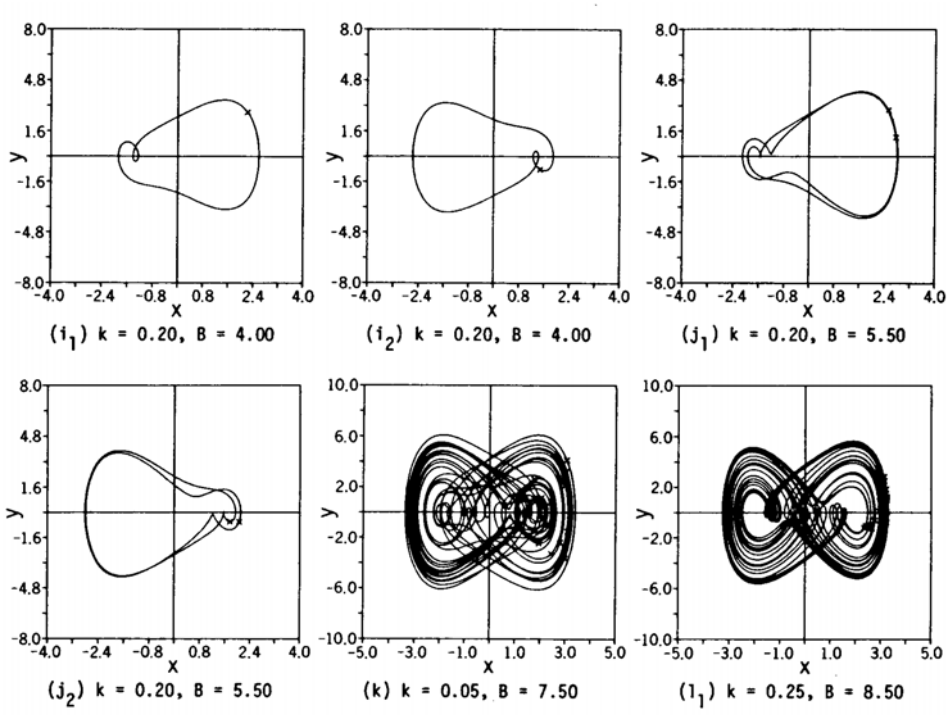

Figure 2. Trajectories of various steady motions in the phase plane for different values of parameters.

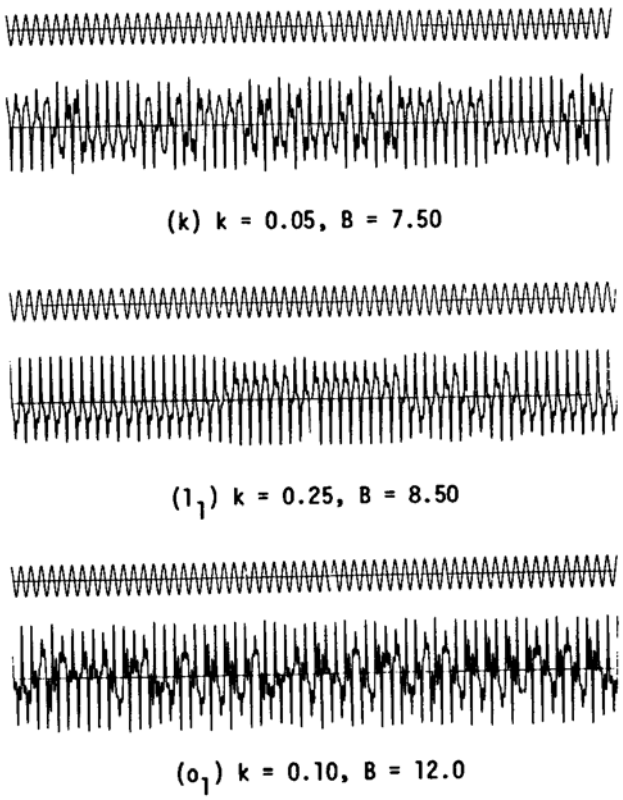

Figure 3. Sample time histories of the response of Duffing's Oscillator.

***Example 2*: Chaotic Vibrations of a Beam with Nonlinear Boundary Conditions**
(F.C. Moon and S.W. Shaw, 1982; F.C. Moon, Chaotic Vibrations, Wiley, 1987)

Consider a cantilever beam with moving boundary and a stop as shown in Figure 4. The beam behaves as a simple cantilever when there is no contact between the beam and the stop. At high amplitude vibrations, however, the motion is constraints by the presence of the stop and the system behaves as a clamped-pinned beam.

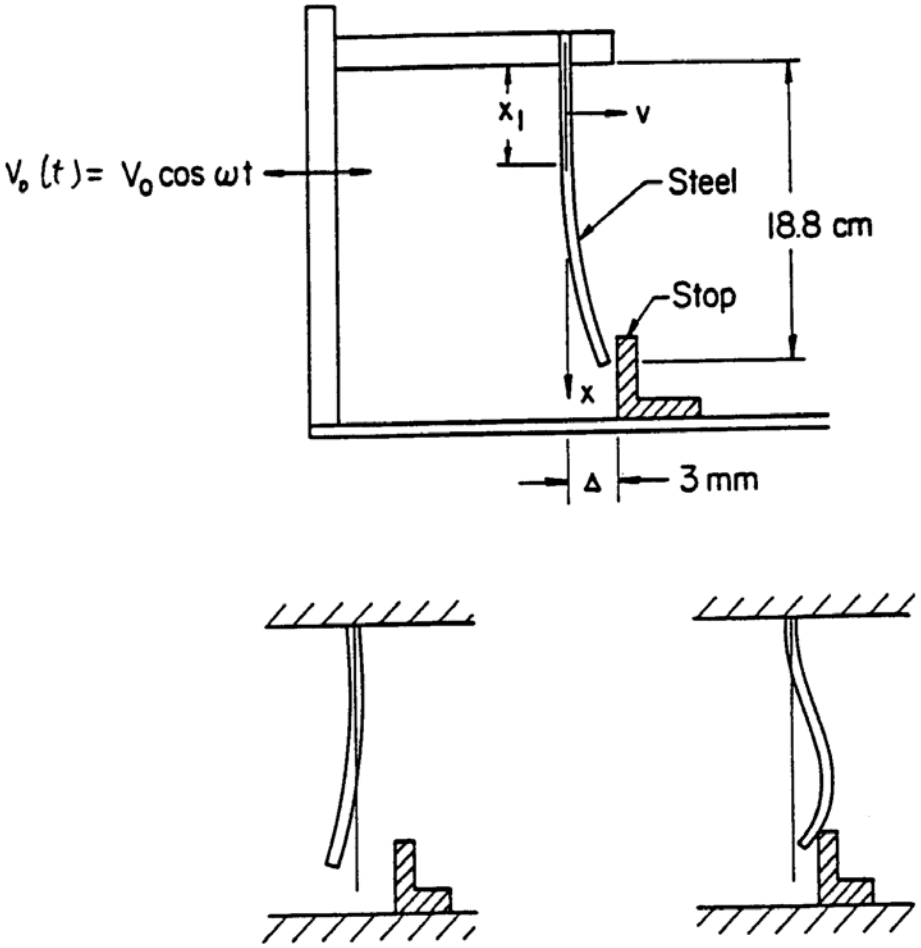

Figure 4. Schematics of the cantilever beam with a stop subject to base excitations.

Equation of Motion:

$$D\frac{\partial^4 v}{\partial x^4} = -\rho\left(\frac{\partial^2 v}{\partial t^2} + \ddot{V}_0\right)$$

where D is the bending stiffness constant of the beam and ρ is mass density.

Model Solutions: $\varphi_i(x) = \cosh\frac{\lambda_i x}{L} - \cos\frac{\lambda_i x}{L} - \alpha_i\left(\sinh\frac{\lambda_i x}{L} - \sin\frac{\lambda_i x}{L}\right)$

$i = 1$ (cantilever) $\lambda_1 = 1.875, \quad \alpha_1 = 0.7341$

$i = 2$ (clamped-pinned) $\lambda_2 = 3.927, \quad \alpha_2 = 1.0008$

Noting that $\varphi_1(L) = 2$, solution is given by

$$v(x,t) = a_1(t)\varphi_1(x) \quad \text{for} \quad a_1 < \frac{\Delta}{2},$$

$$v(x,t) = \frac{\Delta}{2}\varphi_1(x) + a_2(t)\varphi_2(x) \quad \text{for} \quad a_2 > 0.$$

Let

$$a(t) = \begin{cases} a_1(t) & a_1 < \dfrac{\Delta}{2} \\ \dfrac{\Delta}{2} + a_2(t)\varphi_2(x_1) & a \geq \dfrac{\Delta}{2} \end{cases}$$

where we have used $\varphi_1(x_1) = 1, \quad x_1 = 0.032L, \quad \varphi_2(x_1) = 1.48.$

Using a Galerkin procedure and the fact that

$$\int_0^L \varphi_i^2(x)dx = L, \qquad \frac{d^4\varphi_i}{dx^4} = \beta_i^4\varphi_i, \qquad \left(\beta_1 = \frac{1.875}{L},\ \beta_2 = \frac{3.927}{L}\right),$$

$$\int_0^L \varphi dx = I_i, \qquad I_1 = \frac{2\alpha_1}{\beta_1}, \qquad I_2 = \frac{\left[\left(\alpha_2^2+1\right)^{\frac{1}{2}} - \left(\alpha_2^2-1\right)^{\frac{1}{2}} + 2\alpha_2\right]}{\beta_2},$$

we find

$$\begin{cases} \ddot{a} + \dfrac{D}{\rho}\beta_1^4 a = -\dfrac{\ddot{V}_0}{L}I_1 & \text{for} \quad a < \dfrac{\Delta}{2} \\ \ddot{a} + \dfrac{D}{\rho}\beta_2^4 a = -\dfrac{\ddot{V}_0}{L}I_2\alpha_1 + \dfrac{D}{2\rho}\left[\beta_2^4 - \beta_1^4\Gamma\varphi_2(x_1)\right] & \text{for} \quad a > \dfrac{\Delta}{2} \end{cases}$$

where

$$\Gamma = \frac{1}{L}\int_0^L \varphi_1 \varphi_2 dx\,.$$

Let

$A = \frac{a}{I_1}$ and use $\tau = t\omega_1$, $(\omega_1 = \beta_1^2 \frac{D}{\rho^{1/2}})$ for time. Equation of motion then becomes

$$\ddot{A} + \gamma \dot{A} + \begin{Bmatrix} 1 \\ \kappa \end{Bmatrix} A = \begin{Bmatrix} 1 \\ 1.48 I_2 / I_1 \end{Bmatrix} \frac{V_0 \Omega^2}{L} \cos \Omega t + \begin{Bmatrix} 0 \\ \frac{\Delta}{2I_1}(\kappa - 1.48\Gamma) \end{Bmatrix}$$

where a damping term is added and

$$\kappa = \left(\frac{\beta_2}{\beta_1}\right)^4, \qquad \Omega = \frac{\omega}{\omega_1}, \qquad \gamma \text{ is the damping coefficient.}$$

In the equation of motion, the upper values in the bracketed terms are used for $A < A_0 = 2\Delta I_1$, and the lower values are used for $A > A_0$. Moon and Shaw (1982) suggested the following numerical values for the parameters:

$$\kappa = 19.3, \qquad \frac{1.48 I_2}{I_1} = 1.65, \qquad A_0 = 0.0106, \qquad \gamma = 0.05$$

For small Amplitude Oscillation ($A < A_0$), $\omega_1 = 1$. For very large amplitude oscillation, the frequency approaches the limit

$$\omega_2 = \frac{2\kappa^{1/2}}{1 + \kappa^{1/2}}$$

The equivalent force-displacement relation, the phase plane orbits and the undamped natural frequency of the beam are shown in Figure 5. Moon and Shaw (1982) performed a series of computer simulations and also experimentally measured the beam responses. Figure 6 provides a sample comparison of their experimental and computer simulation responses. The beam response is clearly asymmetric due to the imposed constraint. The general features of the experimental response are well represented by computer simulation.

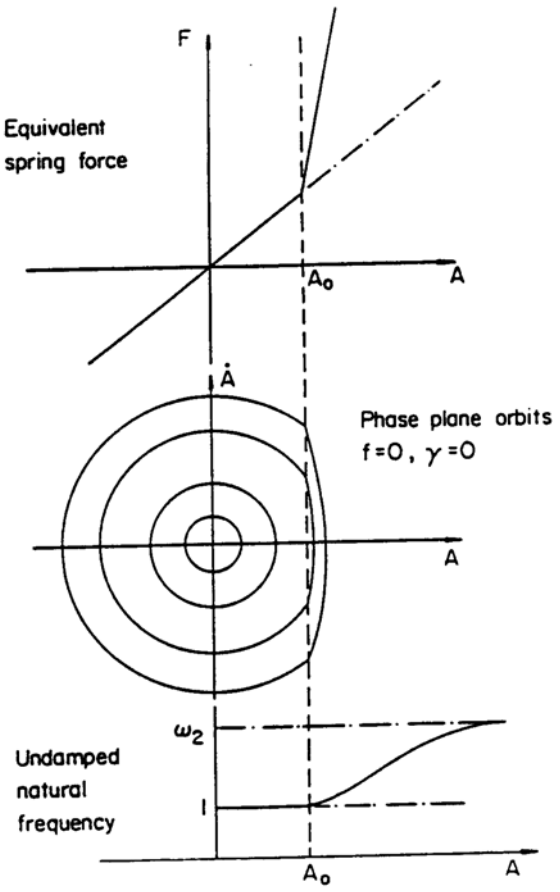

Figure 5. The equivalent force-displacement relation, the phase plane orbits and the undamped natural frequency of the beam.

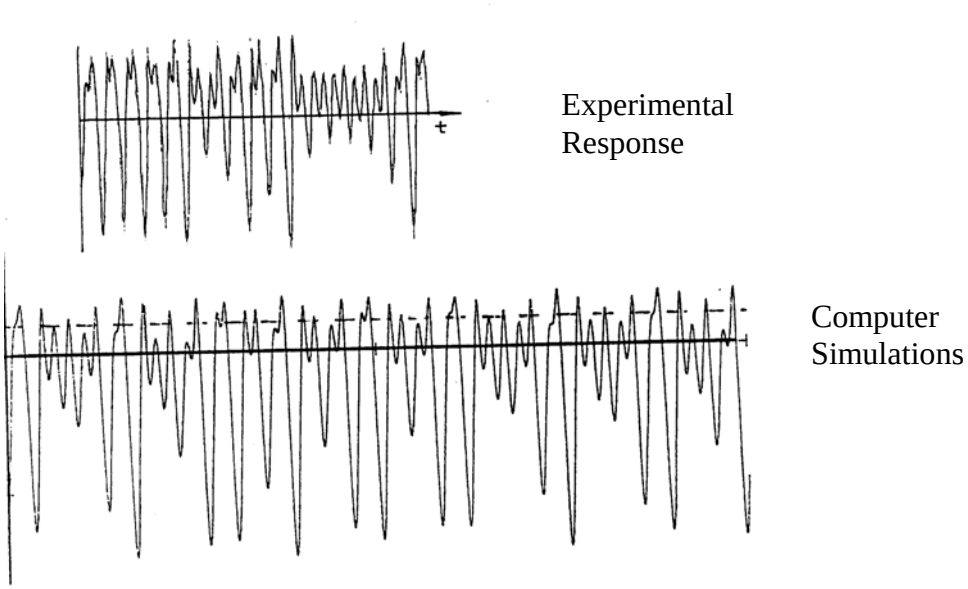

Figure 6. Comparison of experimental and computer simulation responses of the beam (Moon and Shaw, 1982).

***Example 3*: Lorenz Model** (Bender and Orszag (1978), McGraw-Hill)

The Lorenz model is a third-order autonomous system given by

$$\begin{cases} \dfrac{dx}{dt} = -3(x - y) \\ \dfrac{dy}{dt} = -xz + rx - y \\ \dfrac{dz}{dt} = xy - z \end{cases}$$

where r is a constant (controlling) parameter.

When $r < 1$, the only critical (equilibrium) point is at $x = y = z = 0$ and this point is stable. (Evaluation of the critical points and their stability are discussed in the following section.) Hence, for $r < 1$, the system does not exhibit random behavior if $x(0),\ y(0),\ z(0)$ are small.

For $r > 1$, the origin is an unstable critical (stationary) point. In this case, there appear other critical points at $x = y = \pm\sqrt{r-1}$, $z = r - 1$. These critical points are stable if $1 < r < 21$.

For $r > 21$, the critical points at $x = y = \pm\sqrt{r-1}$, $z = r - 1$, and $x = y = z = 0$ are all unstable.

Evaluation of critical (Equilibrium Points)

To find the critical points we set the left-hand side of the differential equation equal to zero and solve for the equilibrium points. That is

$$\left.\begin{array}{c} 3(x - y) = 0 \\ -xz + rx - y = 0 \\ xy - z = 0 \end{array}\right\} \begin{array}{l} \Rightarrow y = x \\ \\ \Rightarrow z = x^2 \end{array}$$

The middle equation now becomes

$$-x^3 + rx - x = 0, \qquad \Rightarrow x = 0,\ x = \pm\sqrt{r-1}$$

Thus, one critical point is $(x = y = z = 0)$, and the others for $r > 1$ are

$$x = \pm\sqrt{r-1},\ y = \pm\sqrt{r-1},\ z = r - 1$$

Stability of the Equilibrium Points

To check the stability, we linearize the equation around the critical point. That is

$$\left\{\begin{array}{c}\dfrac{dx}{dt}=-3(x-y)\\ \dfrac{dy}{dt}=rx-y\\ \dfrac{dz}{dt}=-z\end{array}\right\}$$

where the nonlinear terms are neglected.

We then form the characteristic determinant for the x and y equations. That is we assume $x = Xe^{\lambda t}$ and $y = Ye^{\lambda t}$ in the governing equations and set the determinant of coefficient equal to zero. i.e.,

$$\begin{vmatrix}-3-\lambda & 3\\ r & -\lambda-1\end{vmatrix}=0$$

Note that z is not considered since it gives a stable solution $z = Ce^{-t}$.

The corresponding characteristic equation becomes

$$\lambda^2+4\lambda+3-3r=0$$

with solution being

$$\lambda=-2\pm\sqrt{1+3r}\quad\Rightarrow\quad\left\{\begin{array}{l}r<1\ \Rightarrow\ \text{All}\ \ \lambda's<0,\Rightarrow\text{Stable}\\ r>1\ \Rightarrow\ \text{One}\ \ \lambda>0,\Rightarrow\text{Unstable}\end{array}\right\}$$

Numerical Simulations

Sample results of a series of numerical experiments for a range of parameters are shown in Figures 7-12 (Orzag and Bender, 1978, Mc Graw-Hill).

For $r=17$, critical points are

$$\left\{\begin{array}{l}x=0\\ y=0\\ z=0\end{array}\right\}\quad\text{(Unstable)},\qquad\qquad\left\{\begin{array}{c}x=y=\pm4\\ z=16\end{array}\right\}\quad\text{(Stable)}$$

For an initial condition of x (0) = z(0) = 0, y(0) = 1, Figure 7 shows the time history of y(t) and the phase plane orbit in y-z plane. A regular oscillatory approach to the stable critical point $(-4,-4,16)$ is clearly seen from this figure.

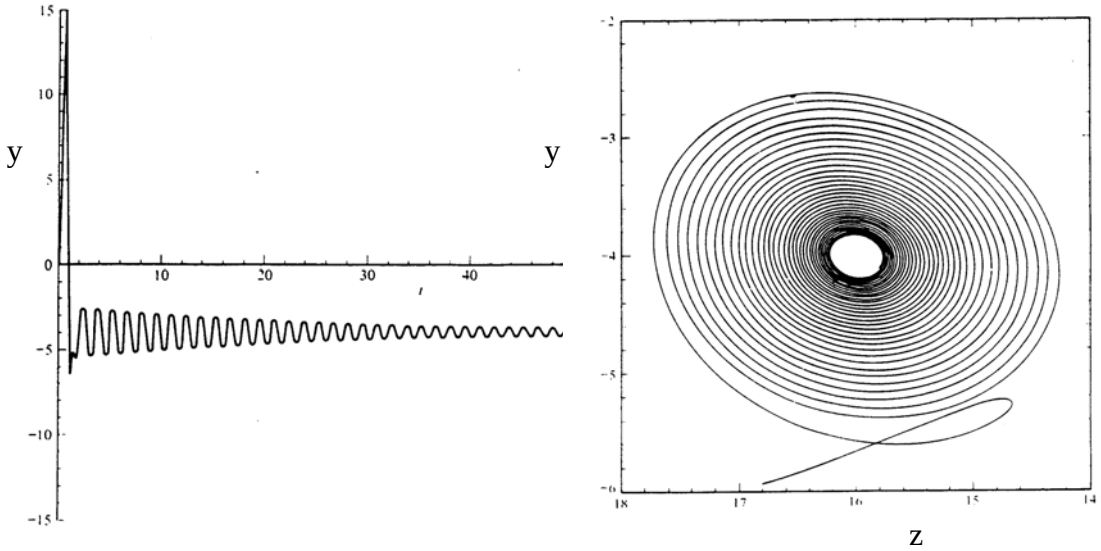

Figure 7. Time history of y(t) and the phase plane orbit in y-z plane for r=17.

For $r = 27$, there are three unstable critical (equilibrium) points. These are

$x = y = z = 0$ (Unstable), $\begin{Bmatrix} x = y = \pm 5 \\ z = 25 \end{Bmatrix}$ (Unstable)

For an initial condition of x (0) = z(0) = 0, y(0) = 1, Figure 8 shows the time history of y(t) and the phase plane orbits in y-x and z-y planes. The chaotic response of the Lorenz model is clearly seen from this figure.

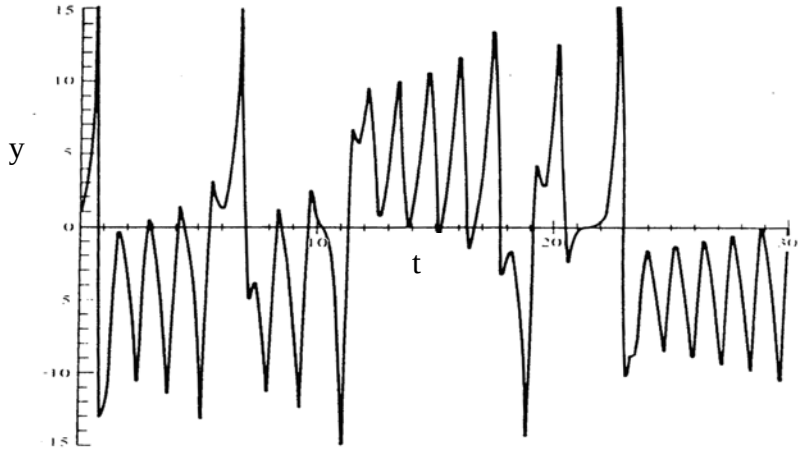

Figure 8. The time history of y(t) for r = 27.

For r=27 and an initial condition of x (0) = z(0) = 0, y(0) = 1, the phase plane orbits of the Lorenz model in y-x and z-y planes are shown in Figure 9. This figure shows that the orbit wanders around the unstable critical points erratically that leads to the chaotic response.

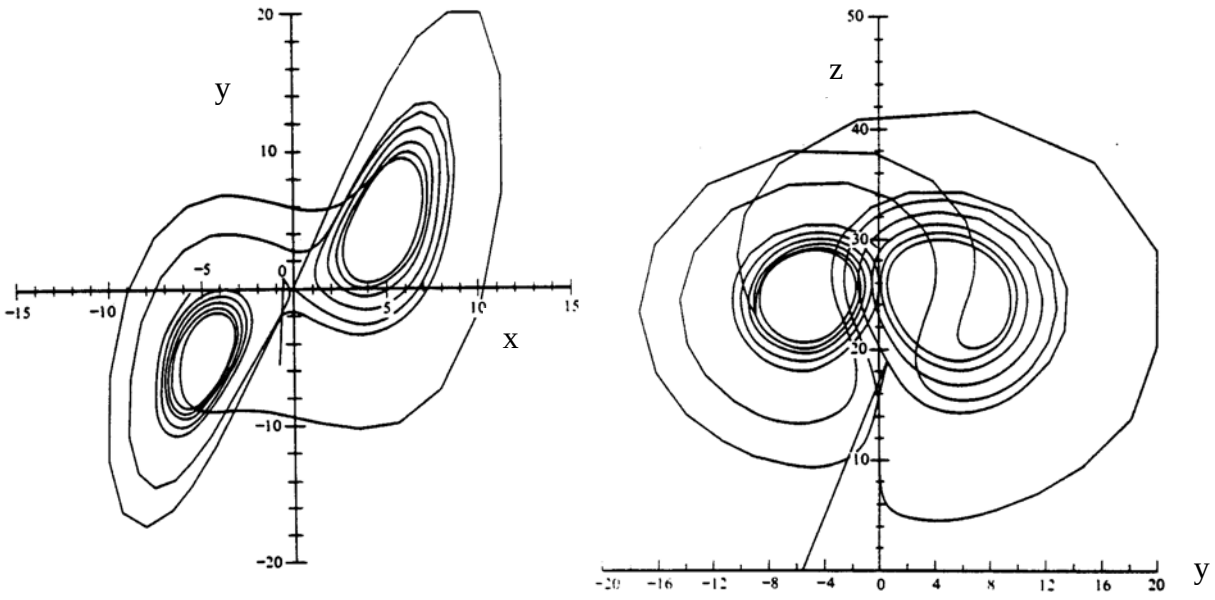

Figure 9. Phase plane orbits for the Lorenz model for r = 27.

Round-Off Error Effects

Figure 10 examines the effect of round-off error on the chaotic response of Lorenz model. Here the simulations are performed using single, double and quadruple precision. While the general features of the chaotic response time histories are quite similar, this figure shows that the time histories evaluated using single precision is quite different from those obtained by double and quadruple precision. The time histories of the double and quadruple precision cases are also somewhat different. Thus, the chaotic response time histories are sensitive to the numerical round-off error. The power spectra shown in Figure 10, however, indicate that the frequency content of the response is not sensitive to the amount of round-off error.

Truncation Error Effects

The effect of truncation error on the chaotic response of Lorenz model is shown in Figure 11. Here the simulations are performed for Δt of 0.00125, 0.0025, 0.005 and 0.01. It is seen that the individual time history varies significantly with the choice of time step. The overall features of the response, however, remain the same. This indicates that the chaotic response is sensitive to the truncation error.

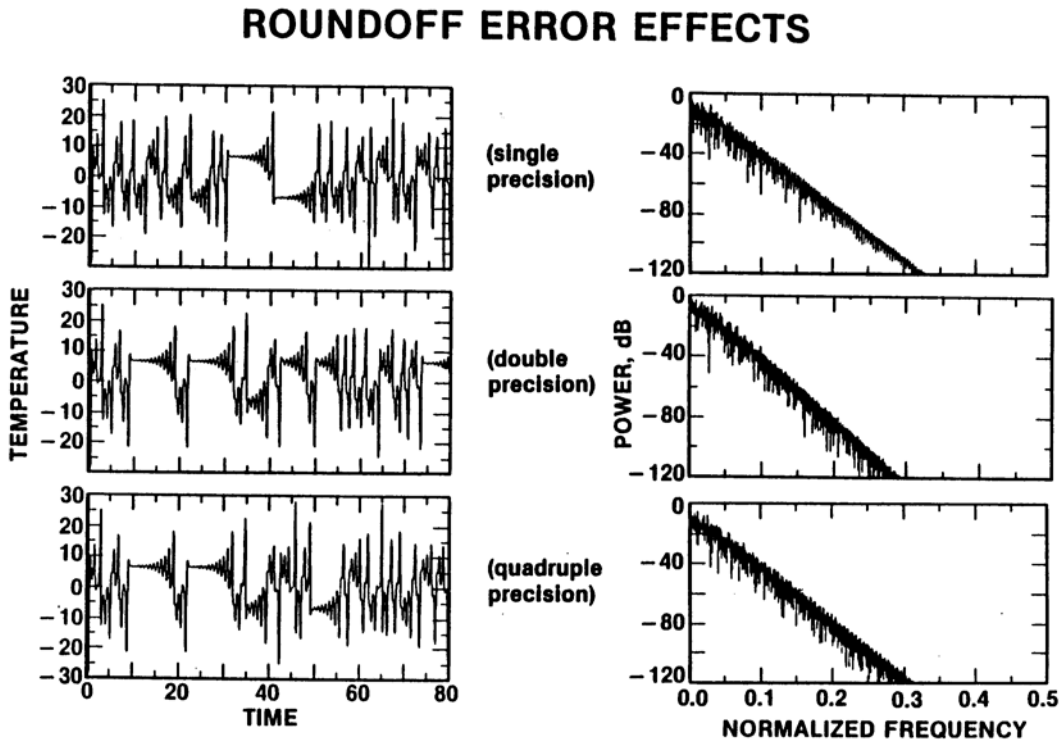

Figure 10. Effect of round-off error on chaotic response of Lorenz model.

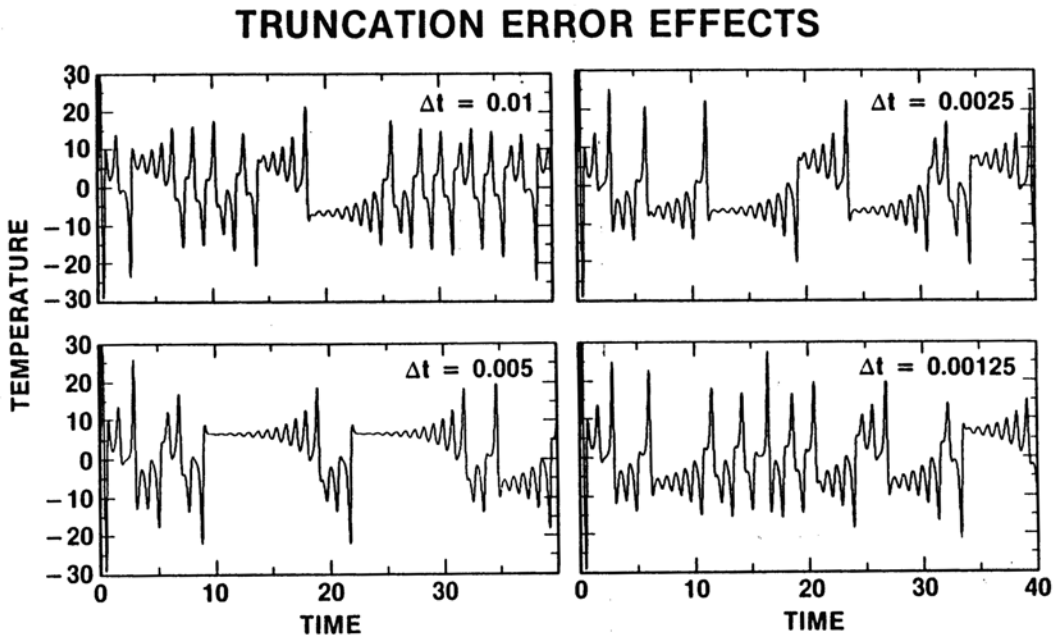

Figure 11. Effect of truncation error on chaotic response of Lorenz model.

The simulation results shown in Figures 10 and 11 imply that computer simulations can predict the statistical features of the time history and the frequency content of the chaotic responses with reasonable accuracy. The precise evaluation of individual time history of the response, however, is difficult due to sensitivity of the system to small perturbations.

***Example 3*: Fifth Order Systems**

Consider a fifth-order system given by

$$\frac{dy_i}{dt} = y_{i+1}y_{i+2} + y_{i-1}y_{i-2} - 2y_{i+1}y_{i-1} \qquad i = 1,2,...,5$$

with $y_i \equiv y_{i+5}$ for all i. The system has an energy integral

$$\frac{d}{dt}\sum_{i=1}^{5} y_i^2 = 0$$

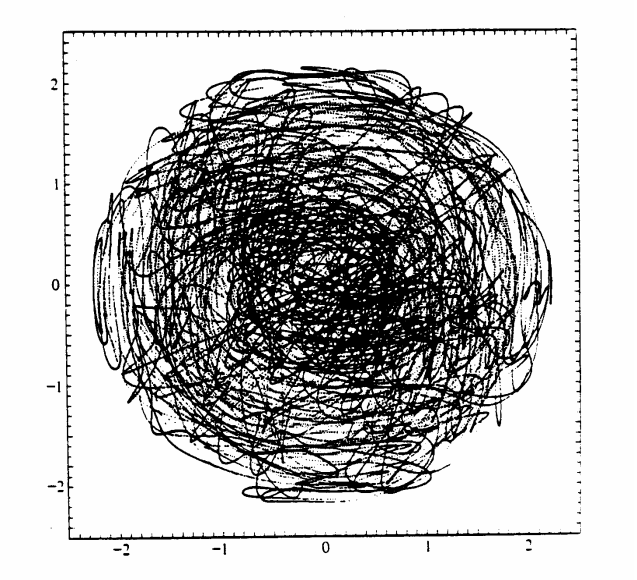

Figure 12. Sample trajectory in y_1y_2-plane.

Chaos in a Double-Diffusive Convection Model in the Presence of Noise (S. A. Abu-Zaid and G. Ahmadi, Appl. Math. Modeling, Vol. 13 (1989)

Mathematical model

The equations describing convection in a horizontal layer of thickness d in the presence of a dissolved solute of concentration S, in the Boussinesq approximation, are

$$\rho_0\left(\partial_t \mathbf{u} + \mathbf{u}\cdot\nabla\mathbf{u}\right) = -\nabla\left(p - p_0\right) + g\left(\rho - \rho_0\right) + \rho\nu\nabla^2\mathbf{u} \tag{1}$$

$$\partial_t T + \mathbf{u}\cdot\nabla T = \kappa_T\nabla^2 T \tag{2}$$

$$\partial_t S + \mathbf{u}\cdot\nabla S = \kappa_S\nabla^2 S \tag{3}$$

$$\nabla\cdot\mathbf{u} = 0 \tag{4}$$

$$\rho = \rho_0\left(1 - \alpha\left(T - T_0\right) + \beta\left(S - S_0\right)\right) \tag{5}$$

where $\mathbf{u}$ is the velocity vector, p is the pressure, T is the temperature, S is the concentration, ρ is the density, κ_S is the solutal diffusivity, κ_T is the thermal diffusivity, α is the coefficient of thermal expansion, β is the corresponding coefficient for salt, and ν is the kinematic viscosity. Here the subscript zero denotes a reference value.

Introducing the stream function ψ with

$$\mathbf{u} = \left(-\partial_z\psi, 0, \partial_x\psi\right) \tag{6}$$

and setting

$$\begin{aligned} T - T_0 &= \Delta T\left(1 - z + \theta\left(x, z, t\right)\right) \\ S - S_0 &= \Delta S\left(1 - z + \Sigma\left(x, z, t\right)\right) \end{aligned} \tag{7}$$

we rewrite equations (1) – (4) as

$$\sigma^{-1}\left[\partial_t\nabla^2\psi + J\left(\psi, \nabla^2\psi\right)\right] = R_T\partial_x\theta - R_S\partial_x\Sigma + \nabla^4\psi \tag{8}$$

$$\partial_t\theta + J\left(\psi, \theta\right) = \partial_x\psi + \nabla^2\theta \tag{9}$$

$$\partial_t\Sigma + J\left(\psi, \Sigma\right) = \partial_x\psi + \tau\nabla^2\Sigma \tag{10}$$

Here

$$J\left(\psi, \theta\right) = \partial_x\psi\partial_y\theta - \partial_y\psi\partial_x\theta \tag{11}$$

$$R_T = \frac{g\alpha\Delta T d^3}{\kappa_T \nu}, \qquad R_S = \frac{g\beta\Delta S d^3}{\kappa_S \nu} \qquad \sigma = \frac{\nu}{\kappa_T} \qquad k = \frac{\kappa_s}{\kappa_T} \tag{12}$$

where R_T is the thermal Rayleigh number, R_S is the solutal Rayleigh number, σ is the Prandtl number, and k is the Lewis number.

We consider the first mode of the flow field and the first two modes of the temperature and concentration fields. That is

$$\psi = 2(2p)^{\frac{1}{2}} \frac{\lambda}{\pi} \sin\frac{\pi x}{\lambda} \sin \pi z \, X(t^*) \tag{13}$$

$$\theta = 2\left(\frac{2}{p}\right)^{\frac{1}{2}} \cos\frac{\pi x}{\lambda} \sin \pi z \, Y(t^*) - \frac{1}{\pi} \sin 2\pi z \, Z(t^*) \tag{14}$$

$$\Sigma = 2\left(\frac{2}{p}\right)^{\frac{1}{2}} \cos\frac{\pi x}{\lambda} \sin \pi z \, U(t^*) - \frac{1}{\pi} \sin 2\pi z \, V(t^*) \tag{15}$$

Substituting the assumed solutions given by (13)-(15) into the governing equations of motion given by (1)-(4), we find

$$\dot{X} = \sigma(-X + r_T Y - r_S U) \tag{16}$$

$$\dot{Y} = -Y + X(1 - Z) \tag{17}$$

$$\dot{Z} = a(-Z + XY) \tag{18}$$

$$\dot{U} = -kU + X(1 - V) \tag{19}$$

$$\dot{V} = a(-kV + XU) \tag{20}$$

where

$$a = \frac{4\pi^2}{p}, \qquad r_T = \frac{\pi^2}{\lambda^2 p^3} R_T, \qquad r_S = \frac{\pi^2}{\lambda^2 p^3} R_S \tag{21}$$

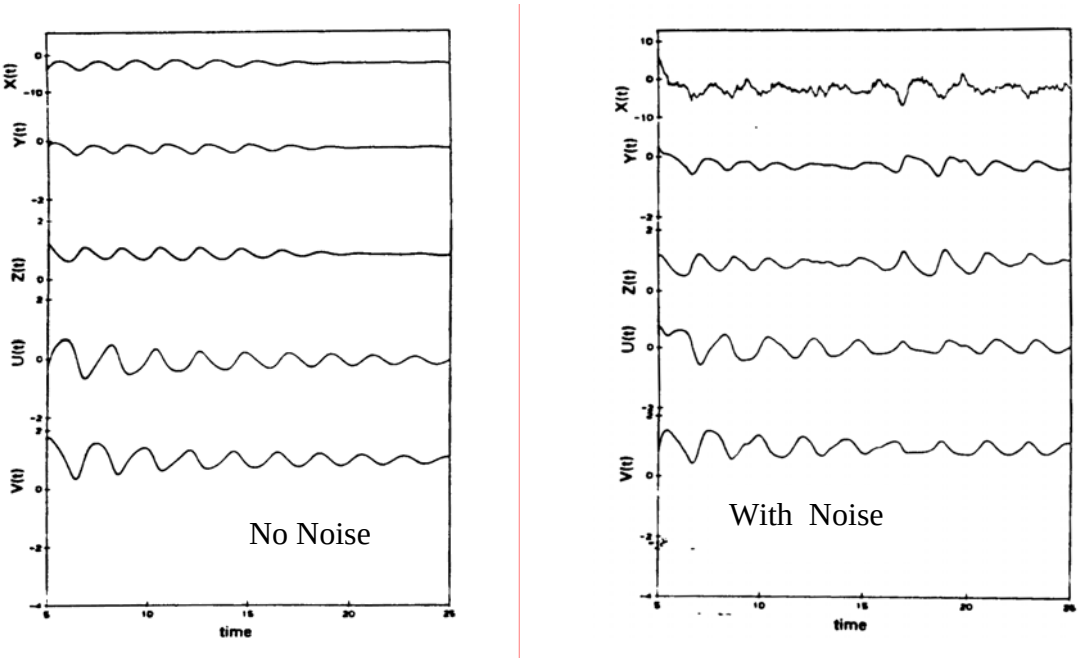

Figure 13. Time variations of modal amplitudes for $r_T = 10$.

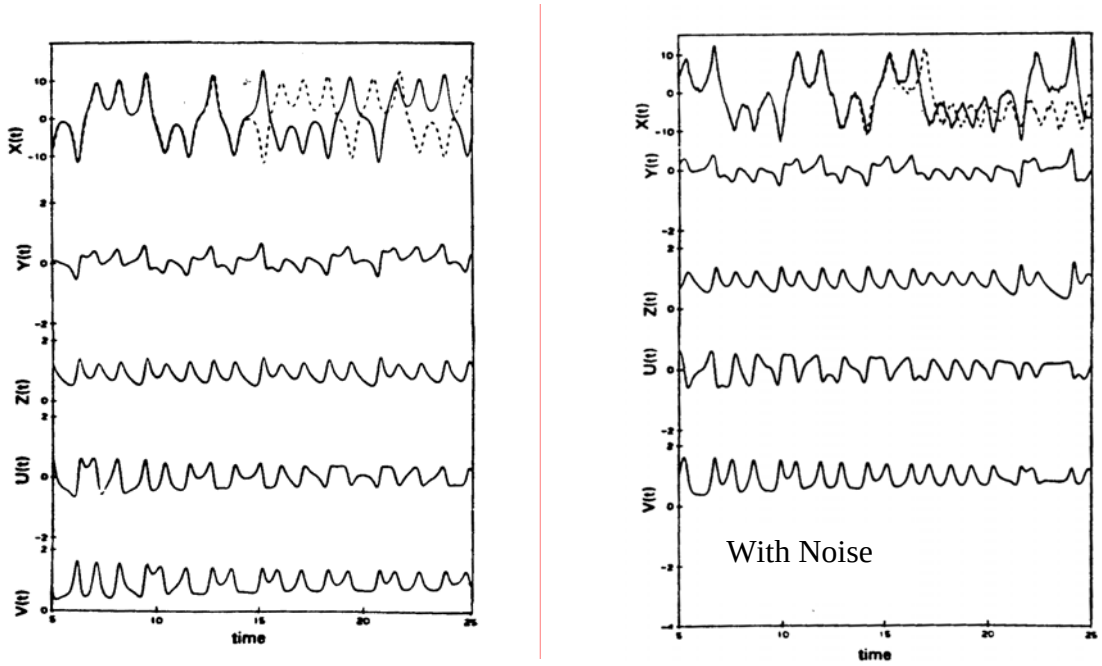

Figure 14. Time variations of modal amplitudes for $r_T = 40$.

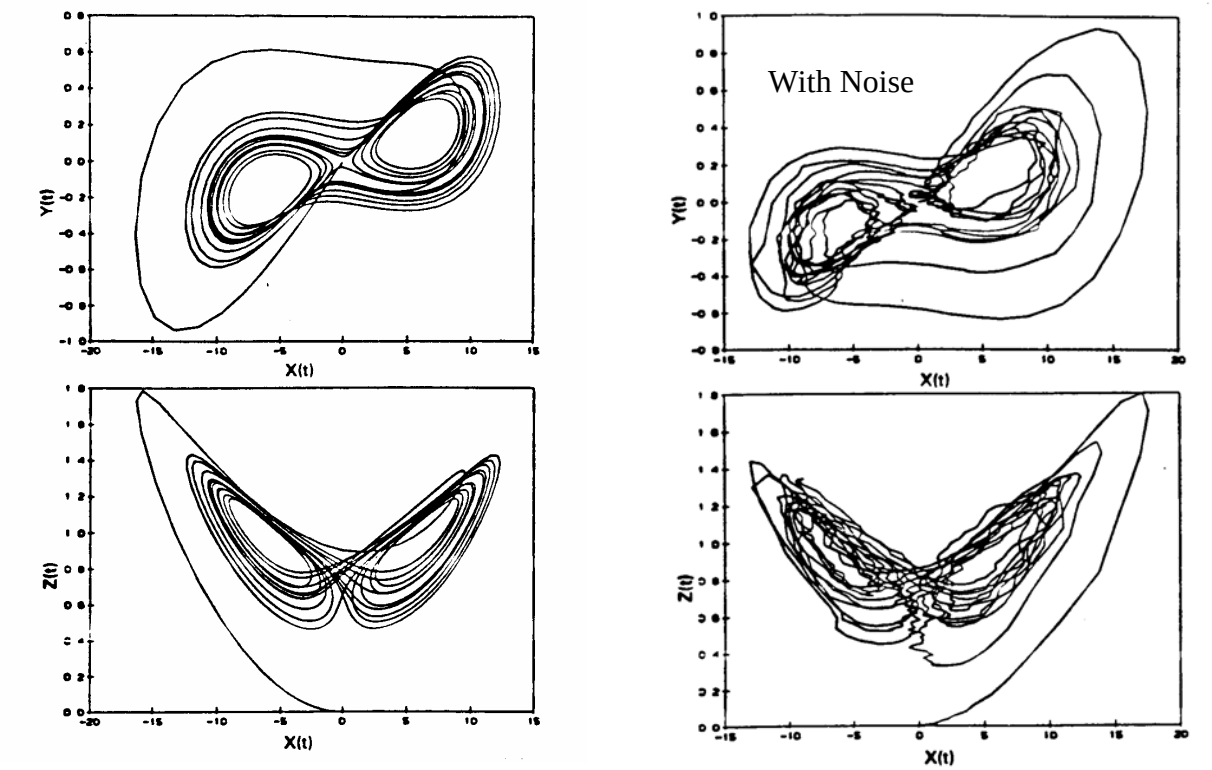

Figure 15. Phase plane orbit for $r_T = 40$ with and without external noise.

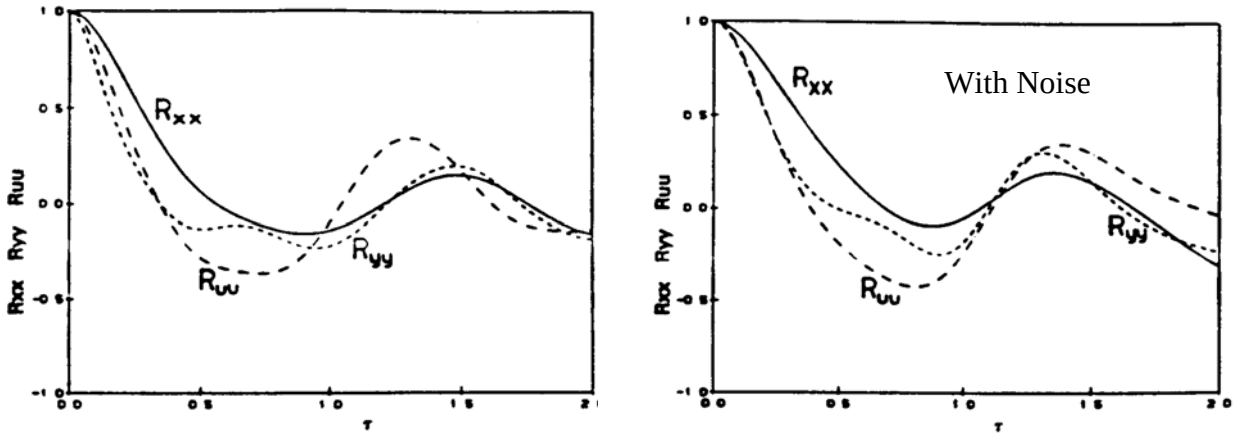

Figure 16. Autocorrelation functions for $r_T = 40$ with and without external noise.

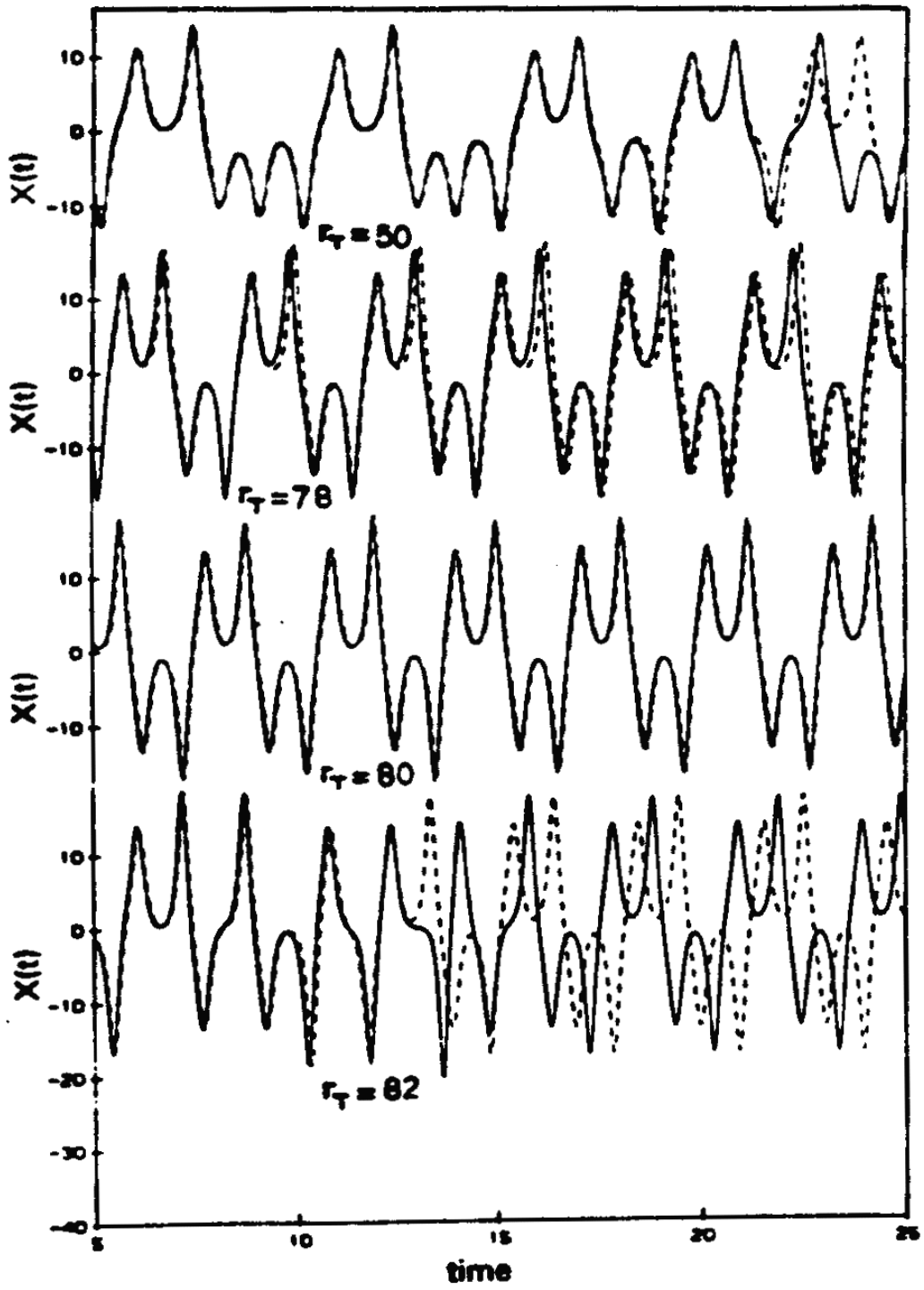

Figure 17. Time histories of the stream function modal amplitude for r_T of 50, 78, 80, 82 and sensitivity to initial condition.

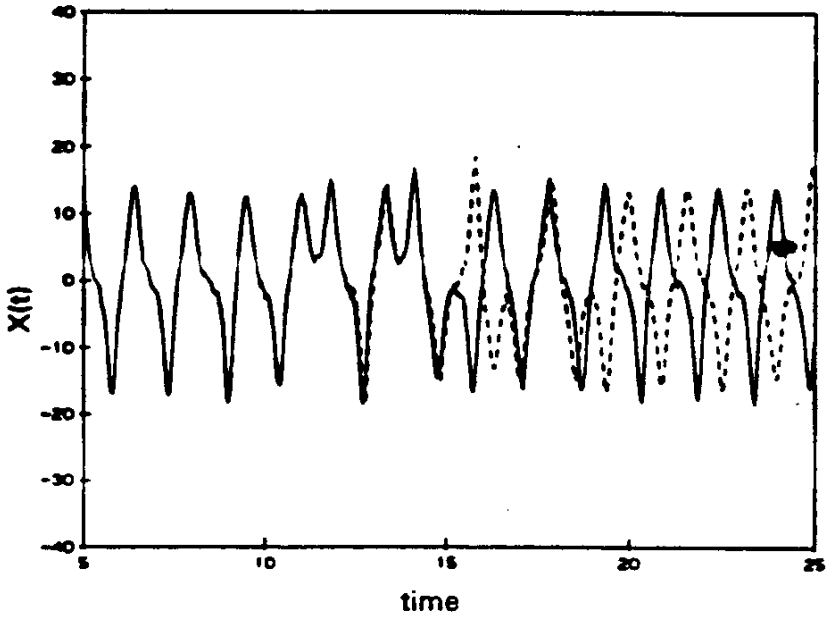

Figure 18. Time histories of the stream function modal amplitude for $r_T = 80$ in the presence of noise and sensitivity to initial condition.

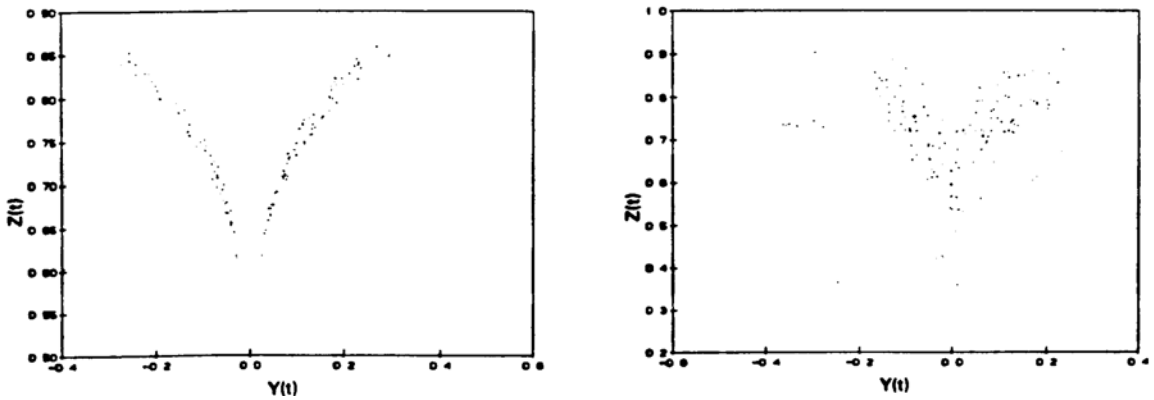

Figure 19. Poincare maps for $r_T = 40$ with and without external noise.

Chaotic Thermal Convection (McLaughlin and Orszag, JFM 1982)

The fluid is assumed to satisfy the Boussineq conditions, so that the governing equations of motion are

$$\frac{\partial \mathbf{v}}{\partial t} = \mathbf{v}\times\boldsymbol{\omega} - \nabla\pi + \mathrm{Pr}\left(\nabla^2\mathbf{v} + \mathbf{k}\theta\right), \tag{1}$$

$$\frac{\partial \theta}{\partial t} + \mathbf{v}\cdot\nabla\theta = \mathrm{Ra}\, w + \nabla^2\theta\ , \tag{2}$$

$$\nabla\cdot\mathbf{v} = 0 \tag{3}$$

where $v = (u, v, w)$ is the velocity field. $\boldsymbol{\omega} = \nabla\times\mathbf{v}$ is the vorticity, $\pi = p + \frac{1}{2}|v|^2$ is the pressure head, with p the pressure, and θ is the deviation of the temperature from the conduction profile. Here

$$\mathrm{Ra} = \frac{g\beta H^3\Delta T}{\nu\kappa} = \text{Rayleigh Number}, \tag{4}$$

$$\mathrm{Pr} = \frac{\nu}{\kappa} = \text{Prandtl Number}, \quad (\mathrm{Pr} = 0.71 \text{ for air}). \tag{5}$$

H is the thickness of the layer and β is the coefficient of thermal expansion.

It is assumed that the velocity and the temperature field can be expanded by a Fourier-Chebyshev series. That is

$$\mathbf{v}(x,y,z,t) = \sum_{|m|<\frac{1}{2}M}\sum_{|n|<\frac{1}{2}N}\sum_{p=0}^{P}\tilde{\mathbf{v}}(m,n,p,t)e^{2\pi i\left(\frac{mx}{X}+\frac{ny}{Y}\right)}T_p(2z), \tag{2.6}$$

$$\theta(x,y,z,t) = \sum_{|m|<\frac{1}{2}M}\sum_{|n|<\frac{1}{2}N}\sum_{p=0}^{P}\tilde{\theta}(m,n,p,t)e^{2\pi i\left(\frac{mx}{X}+\frac{ny}{Y}\right)}T_p(2z), \tag{2.7}$$

Here T_p represents the Chebyshev polynomials and $N = M = P = 16$ is used.

Sample time histories of the velocity field are shown in Figure 20. It is seen that at high Rayleigh numbers the flow becomes chaotic and turbulent.

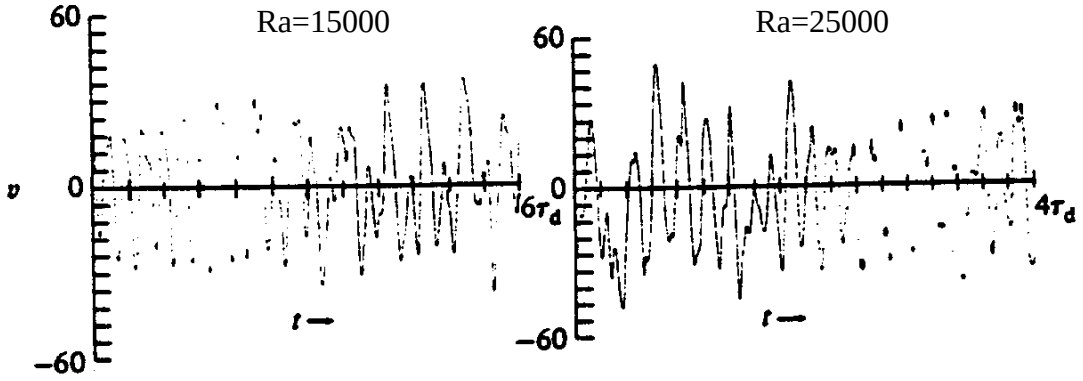

Figure 20. Time histories of the velocity component v(X/4, Y/4, $\sqrt{2}/4$, t for different Rayleigh numbers.

Simulation of a Two-Dimensional Turbulent Flow Field (G. Ahmadi and V.W. Goldschmidt, Developments in Mechanics Vol. 6, 1971)

Direct numerical simulation of two-dimensional isotropic turbulence is performed using a spectral method.

Navier Stokes Equation

$$\frac{\partial \mathbf{u}_f}{\partial t} + \mathbf{u}_f \cdot \nabla \mathbf{u}_f = -\frac{1}{\rho_f}\nabla P + \frac{1}{Re_L}\nabla^2 \mathbf{u}_f \tag{1}$$

$$\nabla \cdot \mathbf{u}_f = 0 \tag{2}$$

The velocity field is expanded into Fourier series given as

$$\mathbf{u}_f(\mathbf{x}, t) = \sum_{\mathbf{K}} \mathbf{u}(K, t) e^{i\mathbf{K}\cdot\mathbf{x}} \tag{3}$$

Introducing the expansion given by (3) into the Navier-Stokes equation given by (1) after some algebra the system of differential equations for the Fourier amplitudes are derived. The resulting systems of coupled differential are truncated and solved numerically on a CDC-6400 computer.

Navier-Stokes Equation in Wave-Vector Space

$$\frac{\partial u}{\partial t}\left(\kappa_x,\kappa_y,t\right)=-\frac{K_x^2+K_y^2}{Re_L}u\left(K_x,K_y,t\right)$$
$$-i\left\{\begin{aligned}&+K_x\left[1-\frac{K_x^2}{K_x^2+K_y^2}\right]\sum_{K_x^1}\sum_{K_y^1}u\left(K_x^1,K_y^1,t\right)u\left(K_x-K_x^1,K_y-K_y^1,t\right)\\&+K_y\left[1-\frac{2K_x^2}{K_x^2+K_y^2}\right]\sum_{K_x^1}\sum_{K_y^1}u\left(K_x^1,K_y^1,t\right)v\left(K_x-K_x^1,K_y-K_y^1,t\right)\\&+K_y\left[\frac{-K_xK_y}{K_x^2+K_y^2}\right]\sum_{K_x^1}\sum_{K_y^1}v\left(K_x^1,K_y^1,t\right)v\left(K_x-K_x^1,K_y-K_y^1,t\right)\end{aligned}\right\}$$
$$\frac{\partial}{\partial t}v\left(K_x,K_y,t\right)=-\left[\frac{K_x^2+K_y^2}{Re_L}\right]v\left(K_x,K_y,t\right)$$
$$-i\left\{\begin{aligned}&+K_x\left[-\frac{K_xK_y}{K_x^2+K_y^2}\right]\sum_{K_x^1}\sum_{K_y^1}u\left(K_x^1,K_y^1,t\right)u\left(K_x-K_x^1,K_y-K_y^1,t\right)\\&+K_x\left[1-\frac{2K_y^2}{K_x^2+K_y^2}\right]\sum_{K_x^1}\sum_{K_y^1}u\left(K_x^1,K_y^1,t\right)v\left(K_x-K_x^1,K_y-K_y^1,t\right)\\&+K_y\left[1-\frac{K_y^2}{K_x^2+K_y^2}\right]\sum_{K_x^1}\sum_{K_y^1}v\left(K_x^1,K_y^1,t\right)v\left(K_x-K_x^1,K_y-K_y^1,t\right)\end{aligned}\right\} \tag{4}$$

Similarly the continuity equation (2) in wave vector space becomes

$$u\left(K_x,K_y,t\right)\cdot K_x+v\left(K_x,K_y,t\right)\cdot K_y=0\,. \tag{5}$$

In these simulation a random Gaussian excitation was imposed to conserve energy.

Figure 21 shows the resulting energy spectrum at the equilibrium condition. The corresponding longitudinal and lateral autocorrelation functions are shown in Figure 22. A sample instantaneous velocity field is plotted in Figure 23.

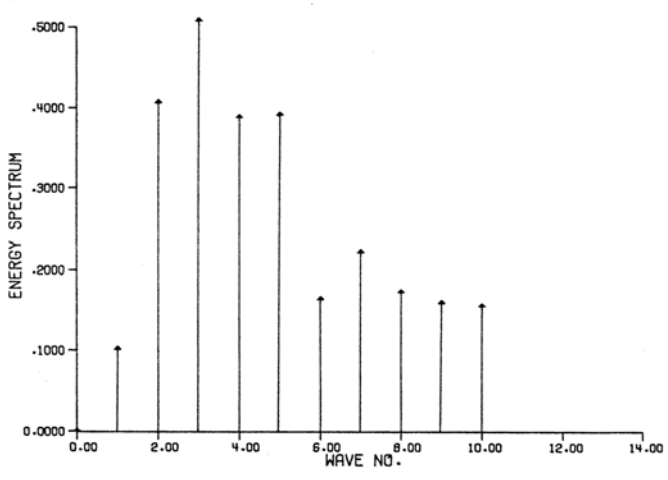

Figure 21. Energy spectrum as a function of wave number.

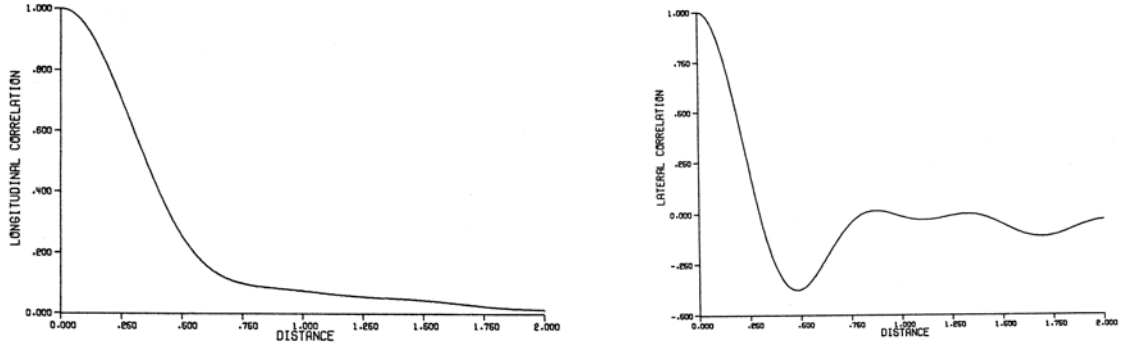

Figure 22. Longitudinal and lateral autocorrelation functions.

Figure 23. An instantaneous velocity contours.

Bifurcation Theory

Bifurcation theory is a theory of equilibrium solutions of nonlinear equations. The motion of a viscous fluid is governed by the Navier-Stokes equation written formally as

$$\frac{\partial \mathbf{u}}{\partial t} = N(\mathbf{u}, Re),$$

where Re is the Reynolds number. By an equilibrium solution, we mean a solution to which $\mathbf{u}$ is evolved after the transient effects associated with the initial values have died away. Equilibrium solutions may be time-invariant, time-periodic, quasi-periodic, or chaotic depending on conditions.

As the Reynolds number is varied, a critical value Re can be reached beyond which the original solution becomes unstable. New solutions, called bifurcating solutions, appear, some of which may be stable and some others may be unstable.

A bifurcation is called supercritical if there is at least one branch of stable bifurcating solutions that is continuous with the original solution at the bifurcating point. Otherwise, it is subcritical bifurcation.

A bifurcation is "regular" if the original time-invariant equilibrium solution is replaced by another time-invariant equilibrium solution. If the original time-invariant solution is replaced by a branch of stable equilibrium solutions which is time-periodic, then the bifurcation is referred to as the "Hopf" bifurcation. A third type of bifurcation occurs if a quasi-periodic solution is replaced by a bounded periodic solution having chaotic character.

Landau-Hopf Theory of Turbulence

Landau-Hopf model views turbulence as a consequence of a countably infinite sequence of bifurcations of solutions to the Navier-Stokes equation. Each bifurcation produces an increasingly complicated quasi-periodic motion of the fluid.

Laudau-Hopf theory lost its credibility in the recent past. While such a flow would present a generally chaotic appearance, it would lack sensitivity to initial conditions. Moreover, its power spectrum would contain well-defined sharp peaks at each of the dominant frequencies, rather than the broad-band noise-type which is the characteristic of turbulent flows.

Strange Attractor Theory of Turbulence (Ruelle-Takens)

Ruelle and Takens proved that the solutions of the Navier-Stokes equation will become attracted to a mathematical structure called a strange attractor after, at most, four bifurcations with respect to the Reynolds number, Re. Such solutions have:

a) Chaotic, but bounded, temporal behavior

b) Extreme sensitivity to initial conditions

Strange attractor can occur in (forced) dissipative nonlinear dynamical systems. A strange attractor can be loosely defined as a subset of solutions all of which are bounded and aperiodic. Each member of this bounded aperiodic set occupies zero volume in the solution space.

Intermittency and coherent structure of turbulence are compatible with the strange-attractor behavior.

Definitions of Turbulent Flows

G.I. Taylor & Von Karman (1937)

"Turbulence is an irregular motion which in general makes its appearance in fluids, gaseous or liquid, when they flow past solid surfaces or even when neighboring streams of the same fluid flow past or over one another."

Hinze (1959)

"Turbulent fluid motion is an irregular condition of flow in which the various quantities show a random variation with time and space coordinates, so that statistically distinct average values can be discerned."